JOURNAL OF MATERIALS SCIENCE 16 (1981) 2774–2780

The use of laser surface melting to homogenize Fe-Al bronzes

C. W. DRAPER
Laser Studies Group, Western Electric, PO Box 900, Princeton, New Jersey 08540, USA

Laser surface melting has been used to homogenize the near-surface region of several Fe–Al bronzes. A continuous CO_2 laser beam was focussed onto the sample surface while the samples moved at high velocities in order to produce melt stripes. The quenched regions were approximately 10 μm deep. In the case of the aluminium bronzes C-61 400 and C-62 400 iron-rich precipitates have been eliminated from the surface region. For C62 400 the pre-irradiation matrix is $\alpha + \gamma_2$, following laser processing, a single phase, presumably metastable β, is formed in the quenched region. The aluminium bronze C-62 500 is not homogenized to the same degree as the C-61 400 or C-62 400. Sample analysis was carried out utilizing optical microscopy, scanning electron microscopy, energy dispersive X-ray analysis and scanning Auger microscopy.

1. Introduction

Laser surface melting (LSM)/quenching is a relatively new and active research area [1–9] in the field of material processing with directed energy sources. Focussed laser energy is used to melt a thin layer with the bulk providing self-quenching. Typical quench rates in metals are of the order of $10^6\,^\circ C\,sec^{-1}$, although the use of Q-switched lasers has recently extended the quench rates accessible to the $10^{10}\,^\circ C\,sec^{-1}$ range [10–12]. Relative motion CO_2 LSM processing has been used to normalize sensitized 304 stainless steel [3], to reduce dealuminification of aluminium bronze in NaCl solutions [4], to increase the incubation period and decrease the erosion rate in the cavitation erosion [5] of 1040 steel, to decrease the susceptibility of titanium alloys to stress corrosion cracking [6], and to increase the hardness of many ferrous alloys [7–9].

One of the explanations [2–5] for the improvement of surface properties is the homogenizing nature of the laser surface melting/rapid quenching operation. The rapid quench rates essentially freeze in liquid-state homogeniety. In this paper we examine the effects of LSM processing on three ternary copper alloys of the aluminium bronze family. An attempt is made to discover to what extent LSM processing can be utilized to homogenize the near-surface region and whether a metastable single phase region can be quenched from the liquid on the multiphase substrate.

2. Experimental procedure

Details of the means by which relative motion CO_2 LSM processing is accomplished appear elsewhere [13]. Briefly, the focussed output of a CW CO_2 laser was used to melt a stripe on copper alloy samples rotating under the beam at high velocity. Area coverage (overlapping individual melt stripes) was achieved by slow translation in combination with high rotation speed. Fig. 1 is a schematic diagram of the LSM processing apparatus. Inert gases (Ar or N_2) were blown through a nozzle assembly, which houses the focussing optics, onto the melt area. This serves both to suppress plasma formation and inhibit oxidation. A 6.35 cm focal length lens was used to focus the transverse electromagnetic mode (TEM_{00}) laser output to optical spot sizes of approximately 100 μm. The transverse velocity was $100\,cm\,sec^{-1}$ for the C-61 400 samples and $200\,cm\,sec^{-1}$ for the C-62 400 and C-62 500 samples. Incident power densities of 3 to $5 \times 10^6\,W\,cm^{-2}$ were used. Dwell times were of the order of 50 μsec. The resulting melt stripes were approximately 60 μm in width and

 0022–2461/81/102774–07$02.70/0

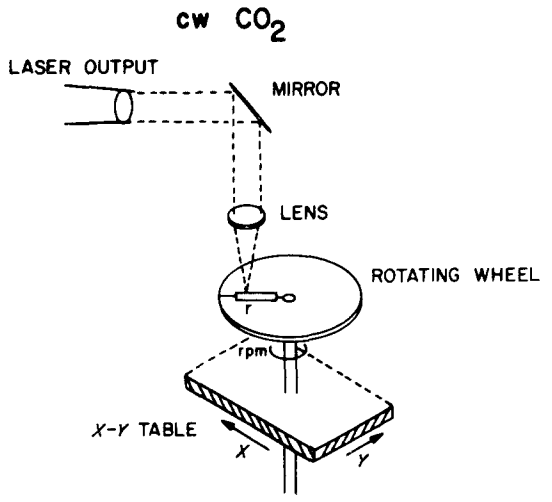

Figure 1 Schematic diagram of laser surface melting apparatus.

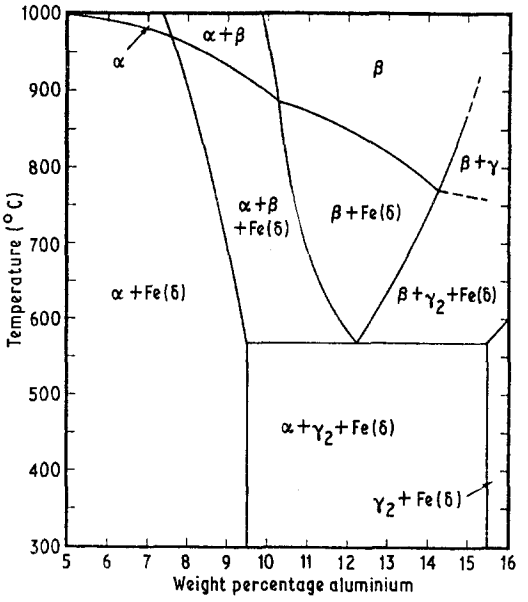

Figure 2 Vertical section at 3 wt% Fe of the Cu–Al–Fe phase diagram.

10 μm deep. Table translation and wheel rotation were such that a 30 to 50% overlap occured between subsequent melt stripes.

Flat samples approximately 4 cm^2 in area and 1 mm in thickness were cut from the as-received stock. These were polished to a 600 grit finish and cleaned ultrasonically in detergent, purified water and spectroscopic grade methanol. The chemical compositions and microstructures of the samples are given in Table I.

3. Results

Following LSM processing, sample surfaces were examined with optical microscopy (OM), scanning electron microscopy (SEM), energy dispersive X-ray elemental mapping (EDAX) and scanning Auger microscopy (SAM). Longitudinally cross-sectioned samples were polished metallographically, etched and examined by OM, SEM and EDAX.

A vertical section of the Cu–Al–Fe system at 3 wt% Fe is given in Fig. 2. The results for each alloy will be discussed separately.

3.1. C-61 400

The unirradiated microstructure of the C-61 400 is α(f c c) with iron-rich δ(b c c) precipitates dispersed randomly throughout the matrix. Fig. 3 presents an optical micrograph of a cross-sectioned, polished and etched (ammonium persulphate) sample which has been LSM processed. The melt depth is approximately 10 μm and within that region, which has been rapidly self-quenched from the liquid phase, iron-rich phase precipitation has been suppressed. The precipitates, which are easily identified and readily mapped in the non-LSM

TABLE I Composition and microstructure of ternary copper alloys prior to laser irradiation

Unified numbering system designation	Trade name	Fabrication	Composition (wt%)	Impurities (each < 0.1%)	As-received microstructure
C-61 400	Aluminium bronze D	DC cast, cold rolled	Cu-90.01, Al-6.30, Fe-3.68	Ni, Zn	α + Fe(δ)
C-62 400	Ampco 18	Horizontal cast bar	Cu-85.61, Al-10.43, Fe-3.64	Zn, Ni, Si, Mn, Sn, Pb, Co, Cr	α + (α + γ_2) + Fe(δ)
C-62 500	Ampco 21	Extruded bar	Cu-81.94, Al-12.54, Fe-4.09, Mn-1.10	Ni, Sn, Si, Co, Zn, Cr	β′ + γ_2 + Fe(δ)

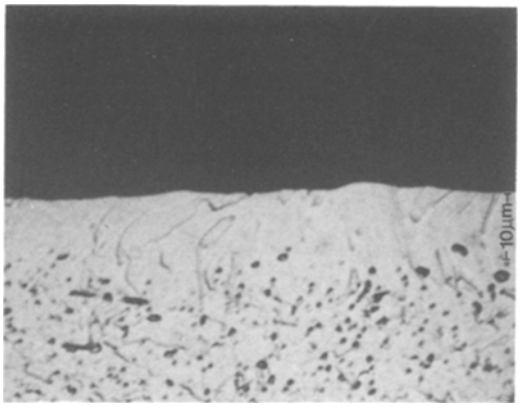

Figure 3 Optical micrograph of a metallographic cross-section of laser surface melted C-61 400 sample. The dark precipitates are the δ-Fe-rich phase.

bulk with SEM/EDAX, cannot be resolved at an instrument magnification limit of 20 000.

Auger spectroscopy has also been used to examine the homogenization resulting from LSM processing of C-61 400. Samples irradiated over approximately 50% of their area were prepared. The sample surface was argon ion sputtered to remove atmospheric oxygen, carbon, nitrogen, sulphur and chlorine contamination. Fig. 4 is a composite of two Auger electron spectra and two SAM elemental maps summarizing the surface analysis. The spectra of Fig. 4a and b were collected from unirradiated α and δ-Fe phases, respectively. The most significant differences are in the Cu and Fe peaks. There is little difference in the Al peak, as one would expect since the concentration of Al is nearly the same in both the α-Cu and δ-Fe-rich phases [14]. SAM elemental maps of Cu (914 eV), before and after laser irradiation, are given in Fig. 4c and d, respectively. The δ-Fe precipitates, which are only 5 wt% Cu, as compared with 90 wt% for the α-Cu matrix, appear as dark (low signal) regions in the Cu (914 eV) elemental map of the unirradiated sample in Fig. 4c. Fig. 4d is an equivalent surface area Cu map from the LSM processed portion of the same sample. There is no evidence of precipitate formation. SAM elemental maps of Fe (648 eV) were also made. They also show complete homogenization of the Fe due to surface melting.

3.2. C-62 400

The unirradiated microstructure of the C-62 400 is composed of a matrix of α(f c c) and the eutectoid α(fcc) + γ_2 (cubic–Cu_9Al_4). The eutectoid is the result of β(b c c) phase transformation. Precipitates of Fe-rich δ(b c c) are distributed throughout the matrix and eutectoid. An optical micrograph of a cross-sectioned, polished and etched (ammonium persulphate) sample is given in Fig. 5. Two half frames are shown with the non-LSM cross-section on the left and LSM cross-section on the right. Again the apparent melt depth is about 10 μm and within that region there is evidence of a transformation from a complex multiphase system to a homogenized metastable phase. Determination of the nature of this metastable phase will require structural analysis.

Although the black-and-white reproduction in Fig. 5 does not strikingly show it, the quenched layer does not etch the same as the bulk alloy. This has been found with other etchants (ferric nitrate, ferric chloride and ammonium hydroxide) as well. There is also evidence of Fe precipitates in the quenched region, primarily near the transformation boundary.

SEM/EDAX examination of the cross-sectioned C-62 400 samples was performed in order to confirm that in fact Fe precipitates were present in the quenched region. Resolvable precipitates that could be mapped with EDAX were found randomly distributed at depths between about 4 and 10 μm from the surface. Auger surface analysis identical to that performed on the C-61 400 sample described above was also used to examine the *atomic surface* of a sputter cleaned C-62 400 sample. Homogenization like that shown in Fig. 4c and d occurs in the case of LSM processed C-62 400 also.

There are two possible explanations for the presence of Fe precipitates in the region where the matrix has been transformed. The first explanation is that the melt depth and transformation depth might be different. Liquid-state diffusion would be required in order to dissolve the precipitates on such a short time scale, but matrix transformation could occur in the solid state. It is not unusual in laser processing of metals to find a heat affected zone (HAZ) of dimensions comparable to the melt depth. A shallower melt depth than that found in the LSM processed C-61 400 is not unreasonable since the C-62 400 sample transverse velocity was twice that of the C-61 400. This cannot be taken as conclusive, however, since direct comparison of melt depths requires equivalent incident power densities, work piece–focal point tolerances [13], normal spectral reflectances and thermal diffusivities.

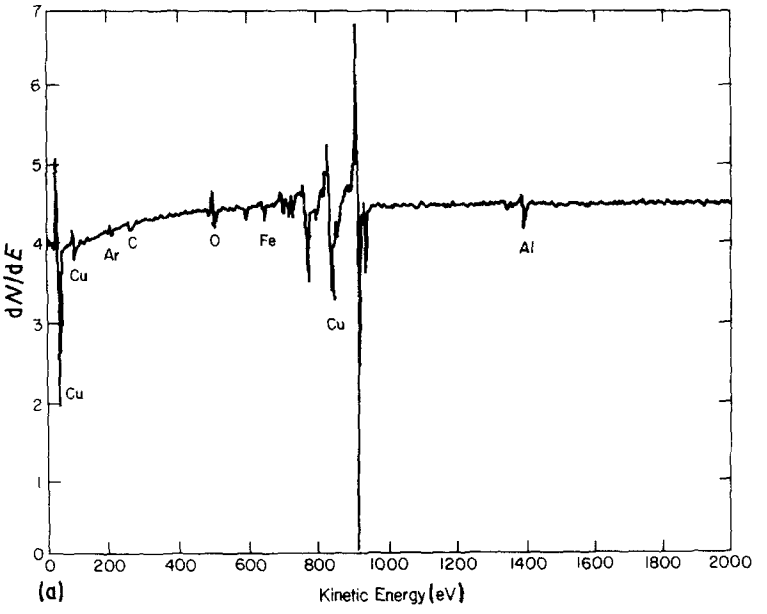

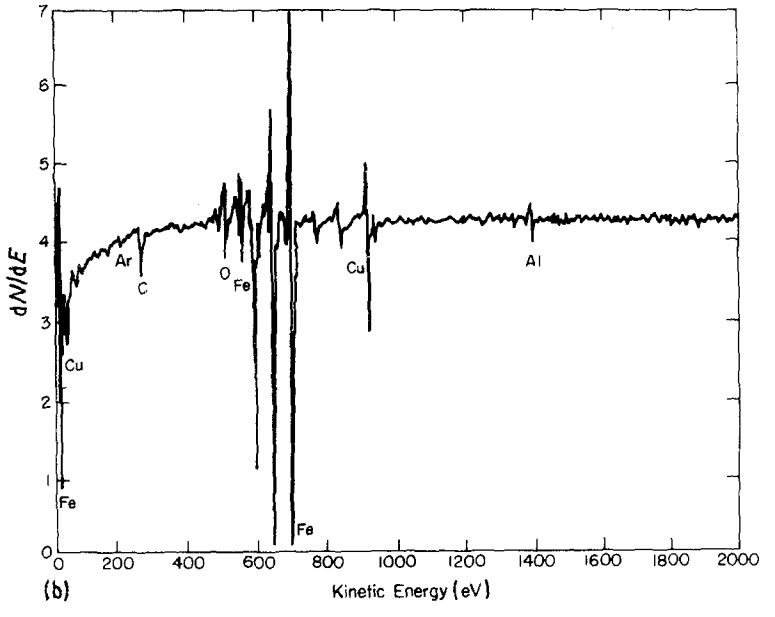

Figure 4 Auger analysis of C-61 400. (a) AES spectrum of α-Cu phase, (b) AES spectrum from δ-Fe precipitate, (c) SAM elemental map of Cu (914 eV) from an unirradiated and sputter cleaned surface. The low signal, dark areas are the δ-Fe phase (d) SAM elemental map of Cu (914 eV) from an LSM processed surface region. Note the absence of Fe precipitates at the atomic surface.

An alternative explanation is that the melt depth and matrix transformation depth are the same, but that, due to shorter time periods in the liquid state for that portion of the melt nearest the extremity of the liquid–solid interface, the precipitates could not be dissolved (convective mixing and diffusion) before the resolidification interface trapped the partially dissolved precipitates on its way back out to the surface. Just such behaviour is seen in the incorporation of transition metal carbides injected into the melt of LSM processed 304 stainless steel [15]. This would imply a gradient or degree of precipitate dissolution as one examined the quenched region from melt edge to surface. Unfortunately, the SEM/EDAX mapping is not sensitive enough to allow definitive measurements to be made.

Examination of the phase diagram in Fig. 2 indicates that for 10.4 wt % Al the melt, upon slow cooling, would pass first through a region of $\beta + \delta$-Fe and then duplex $\alpha + \beta$ plus δ-Fe prior to reaching the eutectoid at about 560° C. One could, therefore, speculate that the quenched matrix may be β', but, as mentioned above, structure analysis

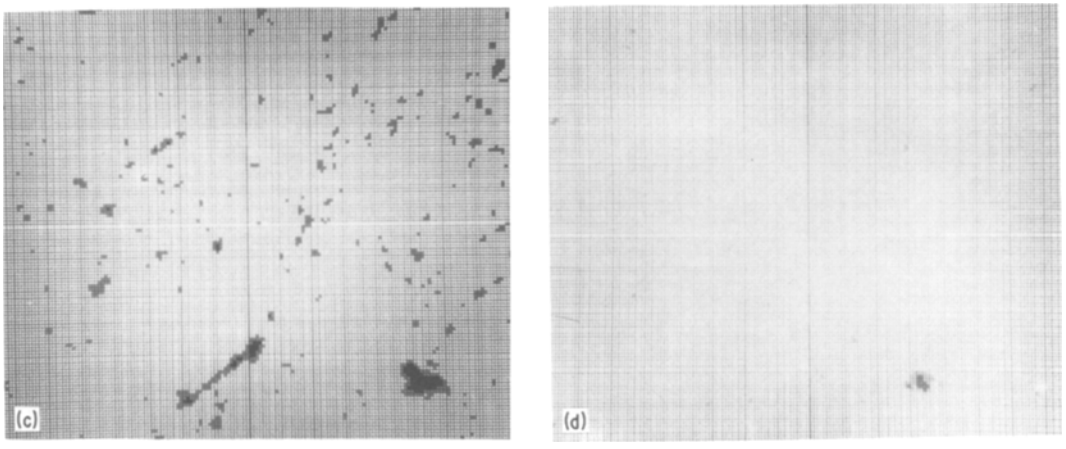

Figure 4 Continued.

will be required to determine the nature of the quenched layer.

3.3. C-62 500

The unirradiated microstructure of the C-62 500 is composed of a matrix of β', that is metastable β(b c c), and γ_2(cubic–Cu_9Al_4), plus, both primary and secondary Fe-rich phases. The role of the 1.1 wt% Mn is to suppress the eutectoid decomposition. An optical micrograph of a metallographic cross-section, etched with ammonium persulphate, is presented in Fig. 6. Again the left-hand portion is a half frame of untreated material, while the right-hand side shows the effect of LSM processing. Only partial homogenization is seen in this case. The two most dominant features seen in the LSM cross-section are the rather large partly transformed grains of γ_2 and primary Fe-rich δ. The influence of convective mixing, which has been identified [16, 17] in many LSM studies in other alloy systems, has grossly distorted the regrowth of the grains. The dynamics of the heat flow are clearly not one-dimensional, that is, normal to the surface with planar melting and regrowth, but involve complex motion between the central melt region and the wings and tail [16, 17] of the scanning melt puddle.

In contrast to the Auger results described above for C-61 400 and C-62 400, elemental Fe mapping of a LSM processed C-62 500 shows evidence for only partial elimination of the Fe in the quenched matrix. Although some homogenization relative to the unirradiated surface has taken place, a significant quantity of Fe has either precipitated from the melt or has never been fully dissolved and homogenized in the liquid during the melt time.

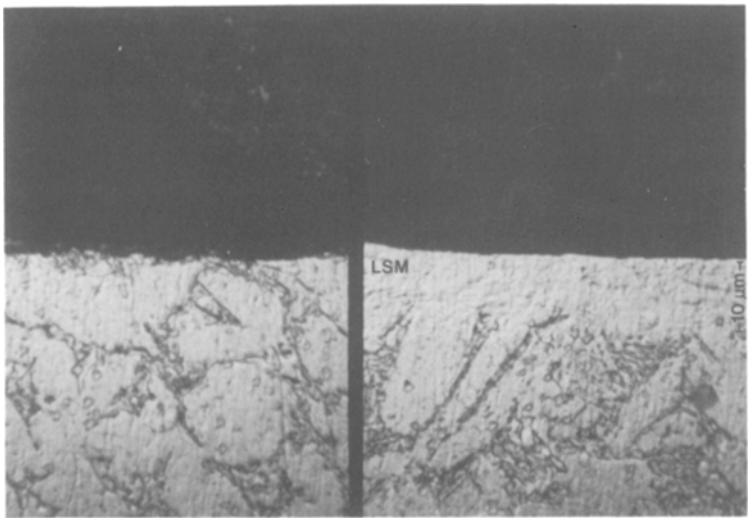

Figure 5 Optical micrograph of a metallographic cross-section of both unirradiated and LSM quenched C-62 400.

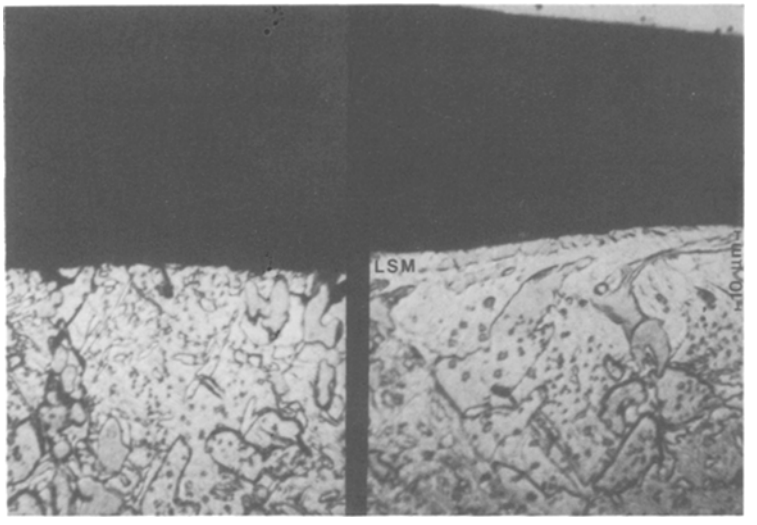

Figure 6 Optical micrograph of a metallographic cross-section of both unirradiated and LSM quenched C-62 500.

Several points are worth noting in attempting to understand these differences in degree of homogenization. First is the fact that the C-62 500 contains rather large, primary Fe-rich phases in addition to the fine precipitate contained in both C-61 400 and C-62 400. Secondly the Fe content is somewhat greater (0.6 wt%) in the case of C-62 500, and finally as in the case of C-62 400 the material transverse velocity during LSM processing was twice that of the C-61 400.

There is some evidence in the optical micrograph of Fig. 6 and in the SAM elemental maps that the fine secondary precipitates have been homogenized while it is the large primary grains which remain after quenching.

Relative to the efficient homogenization seen in the LSM processed C-61 400 and C-62 400 one can summarize the C-62 500 quenched region as being only partially homogenized.

4. Discussion

The sensitivity of the microstructures of aluminium bronzes to various thermal treatments and alloying additions is well documented [18–21]. The presence of γ_2 has been shown to be detrimental to mechanical properties and corrosion resistance and its presence is avoided when possible in commercial alloys either through conventional bulk quenching methods or by specific alloy additions.

The single-phase β region that exists at elevated temperatures, spanning Al contents from about 10 to 14 wt%, makes LSM processing with its associated high quench rates attractive as a method for attempting to retain a single-phase metastable surface. It seems probable that the inefficiency of the homogenization in the case of C-62 500 may be improved somewhat by using greater overlap between successive scans or by repeating the LSM processing several times thus increasing the total time in the liquid phase without changing parameters that effect the actual melt depth or quench rate. Assuming that a homogeneous quenched surface region could be made, and in the case of the C-62 400 where it has apparently been accomplished, structure analysis will be required to determine conclusively the nature of the transformed region.

It is worth noting that the effects of laser surface melting/quenching on some of the surface-sensitive properties of these alloys have been examined. Specifically, the corrosion resistance of C-61 400 in acidic 3% NaCl solutions has been improved following LSM processing [4]. The cavitation erosion resistance of both C-62 400 and C-62 500 have been tested [22] in de-ionized water. Behaviour similar to that reported [5] for LSM processed 1040 steel is observed. There is a significant increase in the incubation period (time to measurable mass loss) and decrease in the erosion rate relative to untreated material. This improvement is seen in spite of the fact that as a result of the LSM processing the surfaces are macroscopically rougher than the unprocessed blanks. Surface roughness has been shown [5, 23] to be detrimental to erosion resistance. There is also little change in hardness, in contrast to the 1040 steel results [5]. The significant improve-

ments in cavitation erosion resistance for the Fe–Al bronzes can be accounted for by the fact that the γ_2 phase has been eliminated in the near-surface region.

5. Summary

It has been demonstrated that different extents of homogenization are accessible through the use of relative motion CO_2 laser scanning in several alloys of the aluminium bronze family. There is some evidence that a matrix transformation which does not require massive compositional diffusion and the dissolution of Fe-rich precipitates which must occur in the liquid phase, may be taking place to varying degrees as a function of depth.

Optical microscopy, SEM/EDAX and scanning Auger microscopy have been used to show that the C-61 400 and C-62 400 LSM processed surfaces are homogeneous single phase. For C-62 500 a partial homogenization is found, but significant quantities of the Fe-rich phase remain. Inspection of the phase diagram indicates that single-phase metastable β should be accessible at these alloy compositions. Structural analysis will be required to confirm the nature of the transformed near-surface regions.

Acknowledgements

The author wishes to acknowledge the technical assistance of J. W. Benko, R. J. Crisci, L. S. Meyer and R. E. Woods. Special thanks to R. E. Willett of Anaconda Research and Technical Centre (C-61 400) and R. J. Severson and Q. F. Ingerson of Ampco Metal (C-62 400 and C-62 500) for both materials, chemical analysis and helpful discussions in relation to the "as-received" microstructures.

References

1. W. A. ELLIOT, F. P. GAGLIANO and G. KRAUSS, *Appl. Phys. Lett.* **21** (1972) 23.
2. E. M. BREINAN, B. H. KEAR and C. M. BANAS, *Phys. Today* **29** (1976) 44.
3. T. R. ANTHONY and H. E. CLINE, *J. Appl. Phys.* **49** (1978) 1248.
4. C. W. DRAPER, R. E. WOODS and L. S. MEYER, *Corrosion, NACE* **36** (1980) 405.
5. C. M. PREECE and C. W. DRAPER, *Wear* **67** (1981) 321.
6. P. MOORE, C. KIM and L. S. WEINMAN, in "Applications of Lasers in Material Processing", edited by E. A. Metzbower (American Society for Metals, Ohio 1979) pp. 259–72.
7. P. R. STRUTT, H. NOWOTNY, M. TULI and B. H. KEAR, *Mater. Sci. Eng.* **36** (1978) 217.
8. F. D. SEAMAN and D. S. GNANAMUTHU, *Met. Prog.* **108** (1975) 67.
9. P. W. CHAN, Y. W. CHAN, F. K. HUI and H. S. NG, *J. Appl. Phys.* **49** (1978) 3634.
10. P. MAZZOLDI, G. DELLA MEA, G. BATTAGLIN, A. MIOTELLO, M. SERVIDORI, D. BACCI and E. JANNITTI, *Phys. Rev. Lett.* **44** (1980) 88.
11. L. BUENE, J. M. POATE, D. C. JACOBSON, C. W. DRAPER and J. K. HIRVOREN, *Appl. Phys. Lett.* **37** (1980) 385.
12. E. RIMINI and J. E. E. BAGLIN, *ibid.* **37** (1980) 481.
13. C. W. DRAPER and J. W. BENKO, *Appl. Opt.* **18** (1979) 3205.
14. J. A. MULLENDORE and D. J. MACK, *Trans. Metall. Soc. AIME* **212** (1958) 252.
15. J. D. AYERS and T. R. TUCKER, *Thin Solid Films* **73** (1980) 201.
16. S. L. NARASIMHAN, S. M. COPELY, E. W. VAN STRYLAND and M. BASS, *Metall. Trans.* **10A** (1979) 654.
17. S. M. COPLEY, D. BECK, O. ESQUIVEL and M. BASS, in "Laser–Solid Interactions and Laser Processing – 1978", edited by S. D. Ferris, H. J. Leamy and J. M. Poate (American Institute of Physics, New York, 1979) pp. 161–71.
18. P. J. MACKEN and A. A. SMITH, "The Aluminium Bronzes", 2nd edn. (Copper Development Association, London, 1966), Ch. 12.
19. J. F. KLEMENT, R. E. MAERSCH and P. A. TULLY, *Corrosion, NACE* **16** (1960) 127.
20. D. M. LLOYD, G. W. LORIMER and N. RIDLEY, *Metals Tech.* 7 (1980) 114.
21. R. HAIMANN and A. KRAJCZYK, *ibid.* 7 (1980) 252.
22. M. GABRIEL, C. M. PREECE, A. M. STAUDINGER and C. W. DRAPER, *IEEE J. Quantum Electron.* **17** (1981), to be published.
23. J. FAUTY, MSc thesis, State University of New York, Stony Brook (1975).

Received 11 February and accepted 23 March 1981.